ELECTRIC MACHINE ANALYSIS AND SIMULATION

While an electrical machine exists for the bulk of its time in the steady state, it is during the brief period of transient, nonstationary, behavior that most of the stresses occur which limit the life of the machine. Because the differential equations of an electrical machine are nonlinear, a closed form solution for many of these transient conditions is impossible, and it is necessary to resort to time domain simulation of the relevant differential equations. The modern era of electrical machine simulation had its beginnings largely through the efforts of Dr. Vannevar Bush of M.I.T. Over 70 years ago, Bush described a device called the integraph which realized continuous integration by a principle related to that of the watt-meter (1). Within a year, Bush's integraph was used in the analysis of the pulsating torques of a synchronous motor–compressor set (2). Hence, simulation techniques for modeling transient behavior of ac machines was under development even before the classic papers of Park (3) and Stanley (4) which developed the basic d–q model of the synchronous and induction machine, respectively. Development of simulation techniques has been ongoing since that time with almost 200 papers identified in a 1974 publication (5).

d–q–0 REPRESENTATION OF THREE-PHASE QUANTITIES

The highly coupled nature of induction and synchronous machines had led to the use of artificial variables rather than actual (phase) variables for the purpose of simulation as well as for visualization. The essence of the nature of the transformation of variables that is utilized can be understood by reference to Fig. 1 which shows three-dimensional orthogonal axes labeled a, b, and c. Consider, for instance, the stator currents of a three-phase induction machine which is, in general, made up of three independent variables. These currents (phase variables) can be visualized as being a single three-dimensional vector (space vector) existing in a three-dimensional orthogonal space, that is, the space defined by Fig. 1. The projection of this vector on the three axes of Fig. 1 produce the instantaneous values of the three stator currents. However, in most cases, the sum of these three currents adds up to zero since most three-phase loads do not have a neutral return path. In this case, the stator current vector is constrained to a plane defined by

$$i_a + i_b + i_c = 0 \tag{1}$$

This plane, the so-called *d–q plane,* is also illustrated in Fig. 1. Components of the current vector in the plane are called the *d–q components,* while the component in the axis normal to the plane (in the event that the currents do not sum to zero) is called the *zero component.* When the phase voltages and phase flux linkages also sum to zero, as is the case with most balanced three-phase loads (including even a salient pole synchronous machine), this same perspective can be applied to these variables as well. The components of the phase current, phase voltage, or phase flux linkage vectors in the d–q–0 coordinate system in terms of the corresponding physical variables are

$$\begin{bmatrix} f_q \\ f_d \\ f_0 \end{bmatrix} = \sqrt{\frac{2}{3}} \begin{bmatrix} 1 & -\frac{1}{2} & -\frac{1}{2} \\ 0 & -\frac{\sqrt{3}}{2} & \frac{\sqrt{3}}{2} \\ \frac{1}{\sqrt{2}} & \frac{1}{\sqrt{2}} & \frac{1}{\sqrt{2}} \end{bmatrix} \begin{bmatrix} f_a \\ f_b \\ f_c \end{bmatrix} \tag{2}$$

where f denotes the current variable i, voltage v, or flux linkage λ.

In the dominant case where the three-phase variables sum to zero (i.e., the corresponding vector is located on the d–q

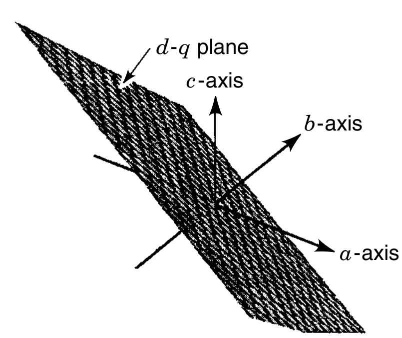

Figure 1. Cartesian coordinate system for phase variables showing location of the d–q plane.

plane), this transformation reduces to

$$\begin{bmatrix} f_q \\ f_d \\ f_0 \end{bmatrix} = \begin{bmatrix} \sqrt{\frac{3}{2}} & 0 & 0 \\ 0 & -\frac{1}{\sqrt{2}} & \frac{1}{\sqrt{2}} \\ 0 & 0 & 0 \end{bmatrix} \begin{bmatrix} f_a \\ f_b \\ f_c \end{bmatrix} \tag{3}$$

where the last row is now clearly not necessary. Figure 2 shows the location of the various axes when viewed from the d–q plane. Note that the projection of the a-phase axis on the d–q plane is considered to be lined up with the q-axis (the a-phase axis corresponds to the magnetic axis of phase a in the case of an electrical machine). The other axis on the plane is, by convention, located 90° clockwise with respect to the q-axis. The third axis (necessarily normal to the d–q plane) is chosen such that the sequence d, q, 0 forms a right hand set. Other notation, using symbols α, β (Clarke's components), is sometimes used to denote these same variables. Also, with the transformation shown, the d-axis is located 90° counterclockwise with respect to the q-axis. These two axes are sometimes interchanged so that the reader should exercise caution when referring to the literature.

When balanced sinusoidal three-phase ac voltages are applied to such a load, it can be shown that the phase voltage vector traces out a circle on this d–q plane with radius $\sqrt{3/2}$ V_{pk} where V_{pk} is the amplitude of the phase voltage. The vector rotates with an angular velocity equal to the angular frequency of the source voltage (377 rad/s in the case of 60 Hz). The current and flux linkage vectors, being a consequence of applying the voltage to a balanced load, also trace out circles on the d–q plane in the steady state. The fact that the length of the vector differs from the amplitude of the sinusoidal variable has prompted methods to correct this supposed deficiency. Specifically, if the transformation of Eq. (3) is multiplied by $\sqrt{2/3}$, a scale change is made in moving from a–b–c to d–q–0 variables. The transformation becomes

$$\begin{bmatrix} f_q \\ f_d \\ f_0 \end{bmatrix} = \begin{bmatrix} 1 & 0 & 0 \\ 0 & -\frac{1}{\sqrt{3}} & \frac{1}{\sqrt{3}} \\ 0 & 0 & 0 \end{bmatrix} \begin{bmatrix} f_a \\ f_b \\ f_c \end{bmatrix} \tag{4}$$

The visualization of vector rotation on the d–q plane has also led to transformations which serve to rotate with these

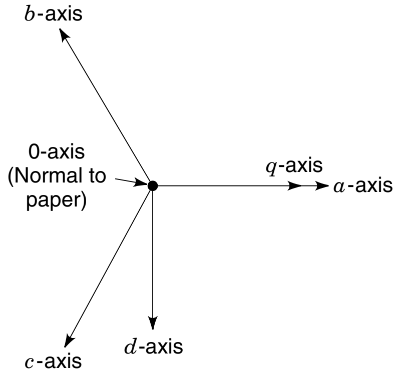

Figure 2. Physical and d–q–0 axes when viewed on the d–q plane.

vectors. For example, if axes are defined which rotate with the stator voltage vector, one realizes the *synchronous voltage reference frame*. In general, it is not necessary to define rotating axes to rotate synchronously with one of the vectors but simply to define a general rotating transformation which transforms the phase variables rotating axes on the d–q plane,

$$\begin{bmatrix} f_q(\theta) \\ f_d(\theta) \\ f_0 \end{bmatrix} = \frac{2}{3} \begin{bmatrix} \cos\theta & \cos\left(\theta - \frac{2\pi}{3}\right) & \cos\left(\theta + \frac{2\pi}{3}\right) \\ \sin\theta & \sin\left(\theta - \frac{2\pi}{3}\right) & \sin\left(\theta + \frac{2\pi}{3}\right) \\ \frac{1}{\sqrt{2}} & \frac{1}{\sqrt{2}} & \frac{1}{\sqrt{2}} \end{bmatrix} \begin{bmatrix} f_a \\ f_b \\ f_c \end{bmatrix} \tag{5}$$

For completeness, the zero component is also given. The scale change of $\sqrt{2/3}$ has also been included. The angle θ is the angular displacement of the vector on the d–q plane measured with respect to the projection of the a-axis on this plane. Since the same scale change has been made for all three components, the zero component uses somewhat unconventional scaling. Specifically, Fortesque's scaling for this component was selected as

$$f_0 = \frac{1}{3}(f_a + f_b + f_c) \tag{6}$$

and is also widely used.

Note that the zero axis does not enter into the rotational transformation. Hence, the zero axis can be considered as the axis about which the rotation takes place, that is, the axis of rotation. Because of the scaling, the power (and subsequently, the torque) is different in d–q–0 components than a–b–c variables, and a 3/2 multiplier must be added to the power in the transformed system of equations since both current and voltage variables have been scaled by $\sqrt{2/3}$.

In vector notation, Eq. (5) can be written as

$$\boldsymbol{f}_{qd0} = \boldsymbol{T}_{qd0}(\theta)\boldsymbol{f}_{abc} \tag{7}$$

where

$$\boldsymbol{T}_{qd0}(\theta) = \frac{2}{3} \begin{bmatrix} \cos\theta & \cos\left(\theta - \frac{2\pi}{3}\right) & \cos\left(\theta + \frac{2\pi}{3}\right) \\ \sin\theta & \sin\left(\theta - \frac{2\pi}{3}\right) & \sin\left(\theta + \frac{2\pi}{3}\right) \\ \frac{1}{\sqrt{2}} & \frac{1}{\sqrt{2}} & \frac{1}{\sqrt{2}} \end{bmatrix} \tag{8}$$

The transformation $\boldsymbol{T}_{qd0}(\theta)$ can, for convenience and for computational advantage, be broken into two portions, one of which takes variables from physical phase quantities to nonrotating d–q–0 variables (stationary reference frame) and then from nonrotating to rotating d–q–0 variables (rotating reference frame). In this case, one can write

$$\boldsymbol{f}_{qd0} = \boldsymbol{T}_{qd0}(\theta)\boldsymbol{f}_{abc} = \boldsymbol{R}(\theta)\boldsymbol{T}_{qd0}(0)\boldsymbol{f}_{abc} \tag{9}$$

where

$$\boldsymbol{T}_{qd0}(0) = \begin{bmatrix} \frac{2}{3} & -\frac{1}{3} & -\frac{1}{3} \\ 0 & -\frac{1}{\sqrt{3}} & \frac{1}{\sqrt{3}} \\ \frac{\sqrt{2}}{3} & \frac{\sqrt{2}}{3} & \frac{\sqrt{2}}{3} \end{bmatrix} \tag{10}$$

and

$$\boldsymbol{R}(\theta) = \begin{bmatrix} \cos\theta & -\sin\theta & 0 \\ \sin\theta & \cos\theta & 0 \\ 0 & 0 & 1 \end{bmatrix} \tag{11}$$

Note that $\boldsymbol{T}_{qd0}(0)$ is obtained by simply setting $\theta = 0$ in Eq. (8). The inverse transformation is

$$\boldsymbol{f}_{abc} = \boldsymbol{T}_{qd0}(\theta)^{-1}\boldsymbol{f}_{qd0} = \boldsymbol{T}_{qd0}(0)^{-1}\boldsymbol{R}(\theta)^{-1}\boldsymbol{f}_{qd0} \tag{12}$$

where

$$\begin{aligned} \boldsymbol{T}_{qd0}(\theta)^{-1} &= \frac{3}{2}\boldsymbol{T}_{qd0}(\theta)^{T} \\ &= \begin{bmatrix} \cos\theta & \sin\theta & \frac{1}{\sqrt{2}} \\ \cos\left(\theta - \frac{2\pi}{3}\right) & \sin\left(\theta - \frac{2\pi}{3}\right) & \frac{1}{\sqrt{2}} \\ \cos\left(\theta + \frac{2\pi}{3}\right) & \sin\left(\theta + \frac{2\pi}{3}\right) & \frac{1}{\sqrt{2}} \end{bmatrix} \end{aligned} \tag{13}$$

$$\boldsymbol{T}_{qd0}(0)^{-1} = \frac{3}{2}\boldsymbol{T}(0)^{T} = \begin{bmatrix} 1 & 0 & \frac{1}{\sqrt{2}} \\ -\frac{1}{2} & -\frac{\sqrt{3}}{2} & \frac{1}{\sqrt{2}} \\ -\frac{1}{2} & \frac{\sqrt{3}}{2} & \frac{1}{\sqrt{2}} \end{bmatrix} \tag{14}$$

$$\boldsymbol{R}(\theta)^{-1} = \boldsymbol{R}(\theta)^{T} = \begin{bmatrix} \cos\theta & \sin\theta & 0 \\ -\sin\theta & \cos\theta & 0 \\ 0 & 0 & 1 \end{bmatrix} \tag{15}$$

*d–q–*0 REPRESENTATION OF THREE-PHASE INDUCTION MACHINES

The benefits of visualizing three-phase variables as a vector represented in a nonphysical coordinate system become apparent only when the system equations of a coupled three-phase magnetic component such as a reactor, transformer, or motor are represented in terms of these newly defined variables. The equivalent circuit of an induction motor represented in a rotating reference frame is shown in Fig. 3. Here, the second subscripts "*s*" and "*r*" are used to denote "stator" and "rotor" quantities, respectively. The enormous simplicity afforded by this equivalent circuit can be better appreciated if it is mentioned that the original circuit defined in physical variables involves the mutual coupling among all six circuits (three stator and three rotor) with 36 consequent mutual and self inductance terms.

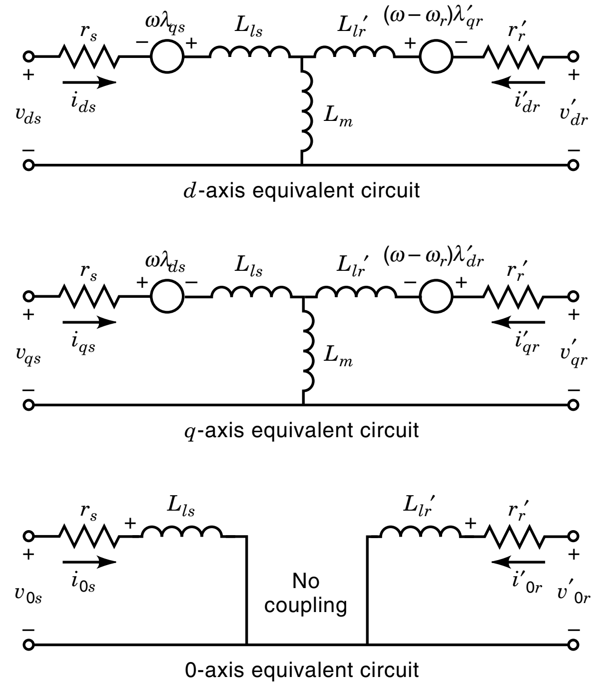

Figure 3. d–q–0 equivalent circuit of an induction machine represented in a rotating reference frame.

Except for notational differences, the parameters in this circuit are essentially the same as the conventional per phase equivalent circuit. That is, r_s, L_{ls}, r_r', L_{lr}', and L_m correspond to the per phase stator resistance, stator leakage inductance, rotor resistance, rotor leakage inductance, and magnetizing inductance, respectively [typically labeled as R_1, L_1, R_2, L_2, and L_ϕ (or L_m) respectively]. In most cases, the impressed rotor voltages are identically zero (squirrel cage machine) and will be assumed henceforth herein as zero. The zero sequence circuits are included for completeness but are seldom necessary and will now also be omitted from further consideration. The primes used for the rotor variables are included as a reminder that the physical variable has been referred to the stator by the stator/rotor turns ratio in much the same manner as for a transformer. The use of these primes is often dropped for convenience.

The voltage generators in the circuit represent speed voltages which appear due to the fact that the circuit is being solved in a rotating reference frame. This term is to be expected of any physical system represented in a rotating frame. (Recall from mechanics the $\omega \times r$ term representing the relative velocity of a stationary point in rotating system.) The speed voltages in the stator portion of the circuit are proportional to the reference frame angular velocity $\omega(\omega = d\theta/dt)$ since the circuits, themselves, are stationary. The speed voltages in the rotor portion are proportional to $\omega - \omega_r$ since the rotor circuits, themselves, are rotating at an electrical angular velocity of $\omega_r(\omega_r = d\theta_r/dt$, where θ_r is the angular rotation of the rotor in electrical degrees). That is, the relative angular velocity appears in this case. The electrical angular displacement is related to the actual physical angular rotor displacement θ_{rm} by $\theta_r = (P/2)\theta_{rm}$, where P is the number magnetic poles of the machine.

The differential equations corresponding to the circuits of Fig. 3 are (neglecting the zero components),

$$v_{qs} = r_s i_{qs} + \frac{d\lambda_{qs}}{dt} + \omega\lambda_{ds} \tag{16}$$

$$v_{ds} = r_s i_{ds} + \frac{d\lambda_{ds}}{dt} - \omega\lambda_{qs} \tag{17}$$

$$v'_{qr} = 0 = r'_r i'_{qr} + \frac{d\lambda'_{qr}}{dt} + (\omega - \omega_r)\lambda'_{dr} \tag{18}$$

$$v'_{dr} = 0 = r'_r i'_{dr} + \frac{d\lambda'_{dr}}{dt} - (\omega - \omega_r)\lambda'_{qr} \tag{19}$$

where the flux linkages λ are defined by

$$\lambda_{qs} = L_{ls} i_{qs} + \lambda_{mq} \tag{20}$$

$$\lambda_{ds} = L_{ls} i_{ds} + \lambda_{md} \tag{21}$$

$$\lambda'_{qr} = L'_{lr} i'_{qr} + \lambda_{mq} \tag{22}$$

$$\lambda'_{dr} = L'_{lr} i'_{dr} + \lambda_{md} \tag{23}$$

and

$$\lambda_{mq} = L_m(i_{qs} + i'_{qr}) \tag{24}$$

$$\lambda_{md} = L_m(i_{ds} + i'_{dr}) \tag{25}$$

Note that while not necessary to be defined explicitly, the mutual (air gap) flux components λ_{mq} and λ_{md} have been included to aid the simulation process.

The torque produced by the machine can be identified as the power consumed by the voltage generators in Fig. 3 divided by the actual rotor speed. Multiplying these voltage generators by their respective currents,

$$T_{em} = \left(\frac{3}{2}\right)\left(\frac{P}{2}\right)\frac{1}{\omega_r}[\omega(\lambda_{ds} i_{qs} - \lambda_{qs} i_{ds}) + (\omega - \omega_r)(\lambda'_{dr} i'_{qr} - \lambda'_{qr} i'_{dr})] \tag{26}$$

$$= \left(\frac{3}{2}\right)\left(\frac{P}{2}\right)(\lambda'_{qr} i'_{dr} - \lambda'_{dr} i'_{qr}) \tag{27}$$

The 3/2 term occurs because of the scale change taken during the d–q–0 transformation. The equation has two useful equivalent forms,

$$T_{em} = \left(\frac{3}{2}\right)\left(\frac{P}{2}\right)(\lambda_{ds} i_{qs} - \lambda_{qs} i_{ds}) \tag{28}$$

or

$$T_{em} = \left(\frac{3}{2}\right)\left(\frac{P}{2}\right)L_m(i'_{dr} i_{qs} - i'_{qr} i_{ds}) \tag{29}$$

Finally, the machine must be physically tied to an external load/prime mover in order to achieve energy conversion. In its simplest form (neglecting mechanical damping), the equation which couples the electrical to the mechanical world can be written

$$T_{em} - T_{\text{load}} = \left(\frac{2}{P}\right) J \frac{d\omega_r}{dt} \tag{30}$$

where T_{load} is the load torque, and J is the inertia in SI units.

SIMULATION OF INDUCTION MACHINE USING FLUX LINKAGES AS STATE VARIABLES

Since the differential equations of the machine, Eqs. (16–19), contain mixed variables (i.e., flux linkages and currents), either of these two quantities could be eliminated from the differential equations by means of the algebraic relations, Eqs. (20–25). The traditional approach to simulation is to consider the flux linkage as the state variables and currents as dependent, algebraically related variables (6). Proceeding in this manner, the currents can be solved in terms of the flux linkages as

$$i_{qs} = \frac{\lambda_{qs} - \lambda_{mq}}{L_{ls}} \tag{31}$$

$$i_{ds} = \frac{\lambda_{ds} - \lambda_{md}}{L_{ls}} \tag{32}$$

$$i'_{qr} = \frac{\lambda'_{qr} - \lambda_{mq}}{L'_{lr}} \tag{33}$$

$$i'_{dr} = \frac{\lambda'_{dr} - \lambda_{md}}{L'_{lr}} \tag{34}$$

$$\lambda_{md} = \frac{1}{\frac{1}{L_{ls}} + \frac{1}{L'_{lr}} + \frac{1}{L_{md}}}\left(\frac{\lambda_{ds}}{L_{ls}} + \frac{\lambda'_{dr}}{L'_{lr}}\right) \tag{35}$$

$$\lambda_{mq} = \frac{1}{\frac{1}{L_{ls}} + \frac{1}{L'_{lr}} + \frac{1}{L_{md}}}\left(\frac{\lambda_{qs}}{L_{ls}} + \frac{\lambda'_{qr}}{L'_{lr}}\right) \tag{36}$$

These results can be inserted into the differential equations. Upon solving for the time derivative terms and integrating, the result is

$$\lambda_{qs} = \int \left[v_{qs} + \frac{r_s}{L_{ls}}(\lambda_{mq} - \lambda_{qs}) - \omega\lambda_{ds}\right] dt \tag{37}$$

$$\lambda_{ds} = \int \left[v_{ds} + \frac{r_s}{L_{ls}}(\lambda_{md} - \lambda_{ds}) + \omega\lambda_{qs}\right] dt \tag{38}$$

$$\lambda'_{qr} = \int \left[\frac{r'_r}{L'_{lr}}(\lambda_{mq} - \lambda'_{qr}) - (\omega - \omega_r)\lambda'_{dr}\right] dt \tag{39}$$

$$\lambda'_{dr} = \int \left[\frac{r'_r}{L'_{lr}}(\lambda_{md} - \lambda'_{dr}) + (\omega - \omega_r)\lambda'_{qr}\right] dt \tag{40}$$

$$\omega_r = \left(\frac{P}{2}\right)\frac{1}{J}\int (T_e - T_{\text{load}})\, dt \tag{41}$$

Equations (28, 31–34) form the necessary equations to simulate a squirrel cage induction machine. A block diagram of showing the flow of information which can be arranged in a suitable simulation language such as MATLAB or ACSL is

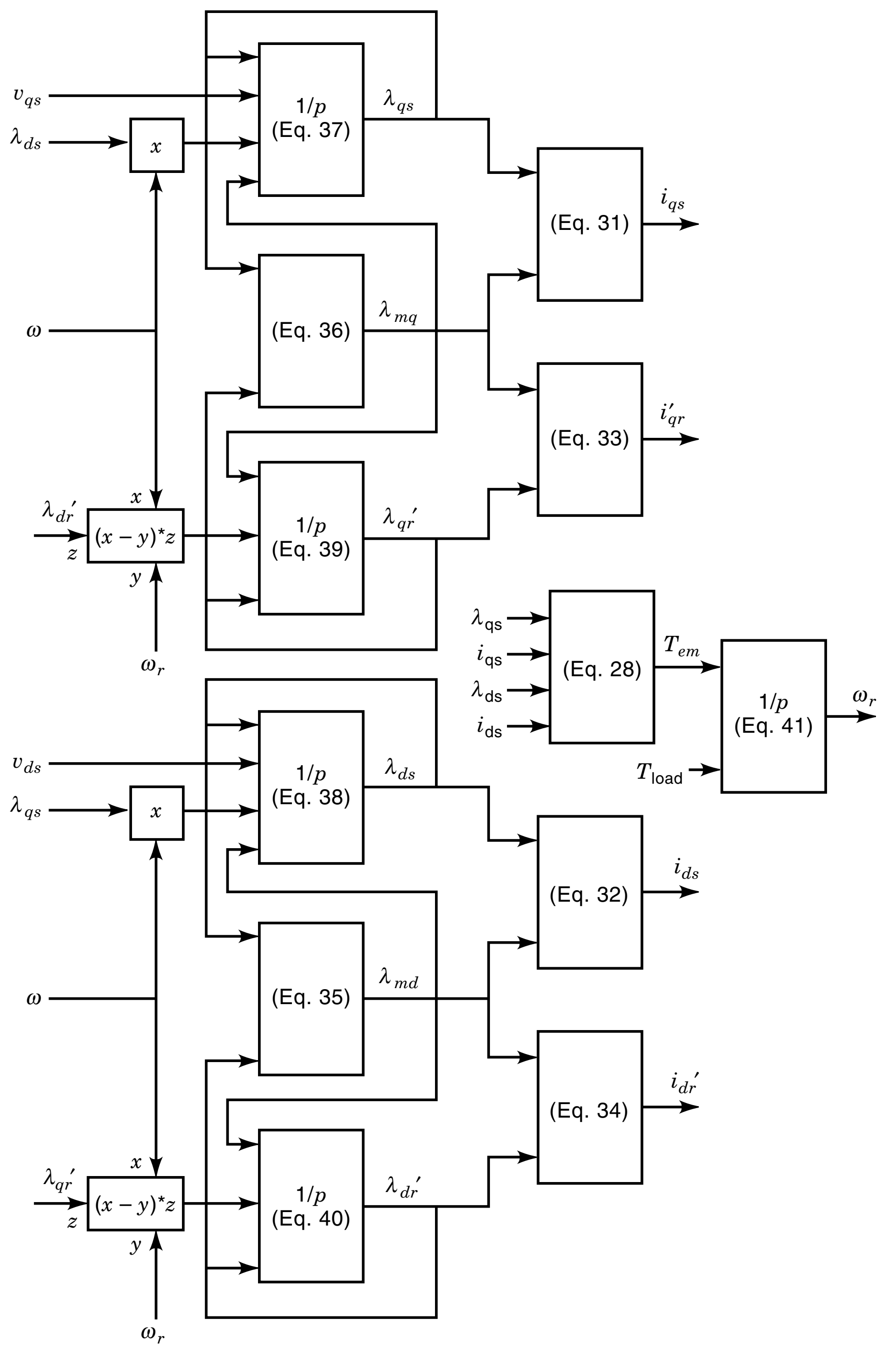

Figure 4. Flow of signals for simulation of a squirrel cage induction machine in a rotating d–q–0 representation.

shown in Fig. 4. The term 1/s denotes integration with respect to time.

While Fig. 4 forms the simulation model of the induction machine, the external inputs, namely v_{qs} and v_{ds}, must be defined. These inputs vary, of course, from problem to problem but can be represented in a general way by the circuit shown in Fig. 5. The voltages e_{ag}, e_{bg}, and e_{cg} are assumed to be known from another portion of the overall system simulation. For example, these three voltages could correspond to the phase to negative dc pole voltages of a three-phase PWM inverter, the output voltages of a generator, or any of a variety of other waveforms obtained either implicitly through simulation or as explicit functions of time. Assuming these voltages as known quantities, the stator phase voltages across the machine are

$$v_{as} = e_{ag} - v_{sg} \tag{42}$$

$$v_{bs} = e_{bg} - v_{sg} \tag{43}$$

$$v_{cs} = e_{cg} - v_{sg} \tag{44}$$

Upon adding these three voltages,

$$v_{as} + v_{bs} + v_{cs} = e_{ag} + e_{bg} + e_{cg} + 3v_{sg} \tag{45}$$

If we let $Z(p)$ denote an arbitrary load impedance which can even be nonlinear provided that it does not vary with stator

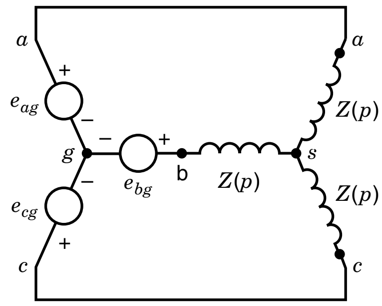

Figure 5. Three-phase wye connection having source voltages determined external to the motor. The point "g" is at an arbitrary (not necessarily ground) potential.

current then, assuming equal impedances in all phases,

$$v_{as} = Z(p)i_{as}$$
$$v_{bs} = Z(p)i_{bs}$$
$$v_{cs} = Z(p)i_{cs}$$

where p denotes the differential operator $p = d/dt$, and $1/p = \int(\cdot)\,dt$ so that

$$v_{as} + v_{bs} + v_{cs} = Z(p)(i_{as} + i_{bs} + i_{cs}) \tag{46}$$

Hence, when the sum of the three load currents equals zero, the sum of the phase voltages also sum to zero. Equation (45) becomes

$$v_{sg} = \frac{1}{3}(e_{ag} + e_{bg} + e_{cg}) \tag{47}$$

While this result has been illustrated for simple passive impedances, it can be shown that the same conclusion is true even if the load is a symmetrical three-phase induction machine or even a salient pole synchronous machine.

The phase voltages can now be solved in terms of the known source voltages as

$$v_{as} = \frac{2}{3}e_{ag} - \frac{1}{3}e_{bg} - \frac{1}{3}e_{cg} \tag{48}$$

$$v_{bs} = -\frac{1}{3}e_{ag} + \frac{2}{3}e_{bg} - \frac{1}{3}e_{cg} \tag{49}$$

$$v_{cs} = -\frac{1}{3}e_{ag} - \frac{1}{3}e_{bg} + \frac{2}{3}e_{cg} \tag{50}$$

or equivalently,

$$\begin{bmatrix} v_{as} \\ v_{bs} \\ v_{cs} \end{bmatrix} = v_{abcs} = \begin{bmatrix} \frac{2}{3} & -\frac{1}{3} & -\frac{1}{3} \\ -\frac{1}{3} & \frac{2}{3} & -\frac{1}{3} \\ -\frac{1}{3} & -\frac{1}{3} & \frac{2}{3} \end{bmatrix} \begin{bmatrix} e_{ag} \\ e_{bg} \\ e_{cg} \end{bmatrix} = \boldsymbol{S}\boldsymbol{e}_{abcg} \tag{51}$$

A block diagram illustrating the procedure for developing the motor d–q voltages is shown in Fig. 6. The two blocks denoted by Eq. (51) and Eq. (10) can be readily solved to form

$$\boldsymbol{T}_{qd0}(0)\boldsymbol{S} = \begin{bmatrix} \frac{2}{3} & -\frac{1}{3} & -\frac{1}{3} \\ 0 & -\frac{1}{\sqrt{3}} & \frac{1}{\sqrt{3}} \\ 0 & 0 & 0 \end{bmatrix} \tag{52}$$

The last row of zeros show that the zero sequence component of voltage is zero. That is, the zero component of voltage is impressed across the open circuit between points s and g and not across the zero sequence circuit of the machine itself

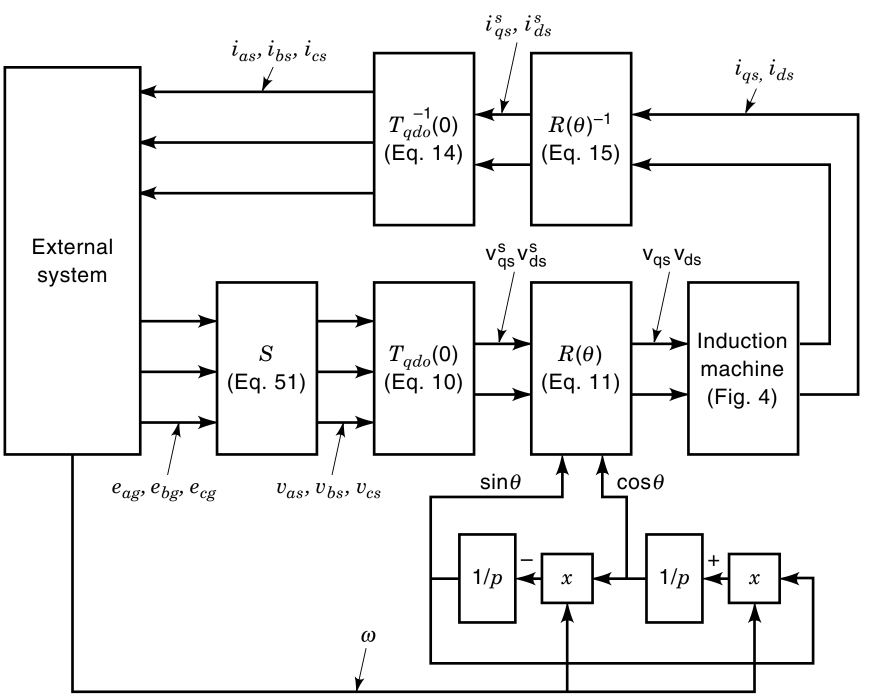

Figure 6. Typical simulation of a wye connected squirrel cage induction machine including modeling of source voltages.

(shown in Fig. 3). In the event that the three source voltages also sum to zero, we have, finally,

$$\boldsymbol{T}_{qd0}(0)\boldsymbol{S} = \begin{bmatrix} 1 & 0 & 0 \\ 0 & -\dfrac{1}{\sqrt{3}} & \dfrac{1}{\sqrt{3}} \\ 0 & 0 & 0 \end{bmatrix} \tag{53}$$

In general, the reference frame velocity can be selected to be any explicit or implicit function of time. The speed of the reference frame is typically chosen to best suit the problem under investigation. For example, if the simulation requires modeling piecewise linear or nonlinear elements such as semiconductor switches, then the reference frame must be constrained to rotate either with the stator or the rotor depending upon where the switches are located. When a simple balanced three-phase sinusoidal operation is investigated, a synchronous reference frame can be used and often adds insight into the problem being investigated. In motor control problems such as field orientation, it is possible to fix the reference frame on a vector corresponding to a variable such as the stator current or rotor flux vector. In the large majority of cases, a simulation in the stationary reference frame, however, suffices in which case θ is constant. If $\theta = 0$, $\boldsymbol{R}$ becomes the identity matrix and can be eliminated since the signals pass directly through the block without modification. In Fig. 6, the reference frame velocity ω is shown as coming from the external system as would be the case if the synchronous voltage rotating reference frame were used. Krause and Thomas (7) give an excellent treatment of simulation techniques to be employed when series connected semiconductor switches open and close, producing temporary open circuit conditions in the phases.

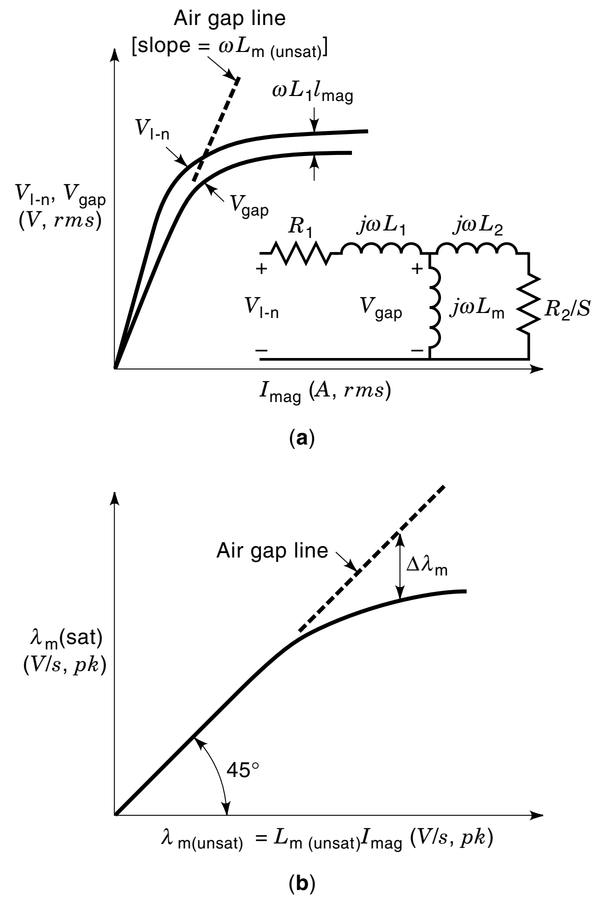

Figure 7. (a) No-load saturation curve. (b) Derived curve.

MODELING OF SATURATION

Probably the most important effect absent from the model developed thus far concerns saturation of the magnetic core. In most cases, the saturation of the teeth dominate, in which case saturation can be taken into account accurately by expressing the air gap flux linkage as a nonlinear function of the air gap MMF. While the air gap MMF is difficult to determine under a loaded condition, the required relationship can be established if the motor is operated under a unloaded condition in which case the MMF is clearly proportional only to the stator current since the rotor current is, in this case, zero. If the no-load voltage is plotted versus the no-load current, the saturation curve of Fig. 7(a) can be established. Neglecting stator resistance, the slope of a line drawn from the origin to a point on the curve is proportional to the sum of the stator leakage plus magnetizing reactance $\omega_e(L_1 + L_m)$, or ($\omega_e(L_{ls} + L_m)$ in d–q notation) where ω_e is the angular frequency of the source voltages. If the leakage reactances of the machine have been measured by locked rotor test or calculated, the voltage drop due to magnetizing current flow in the stator leakage inductance branch can be subtracted from the terminal voltage to obtain the voltage at the air gap. The slope of the air gap voltage versus magnetizing current is clearly the magnetizing reactance $\omega_e L_m$. The slope of the linear portion line (air gap line) yields the unsaturated value of $\omega_e L_{m(\mathrm{unsat})}$. If the abscissa of Fig. 7(a) is multiplied by $L_{m(\mathrm{unsat})}$ and the ordinate by $1/\omega_e$, the normalized curve of Fig. 7(b) results in a new plot in which the abscissa remains proportional to MMF (but scaled in terms of the unsaturated value of flux linkages) and the ordinate equal to the saturated value of flux linkages. The slope at the air gap line is now clearly unity. The difference between the saturated and unsaturated values of flux linkage can be defined as $\Delta\lambda_m$.

The quantity $\Delta\lambda_m$ can now be plotted as a function of the unsaturated value of air gap flux linkages $\lambda_{m(\mathrm{unsat})}$. Since saturation does not result in a phase shift in the fundamental component of flux linkages and only decreases the amplitude, both the d- and q-components of saturated air gap flux should be decreased by the same value. Thus,

$$\Delta\lambda_{md} = \frac{\lambda_{md(\mathrm{unsat})}}{\lambda_{m(\mathrm{unsat})}}\Delta\lambda_m \tag{54}$$

$$\Delta\lambda_{mq} = \frac{\lambda_{mq(\mathrm{unsat})}}{\lambda_{m(\mathrm{unsat})}}\Delta\lambda_m \tag{55}$$

Saturation in the q-axis can be incorporated if Eqs. (20) and (22) are modified to form

$$\lambda_{qs} = L_{ls} i_{qs} + \lambda_{mq(\mathrm{sat})} = L_{ls} i_{qs} + \lambda_{mq(\mathrm{unsat})} - \Delta\lambda_{mq} \tag{56}$$

$$\lambda'_{qr} = L'_{lr} i'_{qr} + \lambda_{mq(\mathrm{sat})} = L_{lr} i_{qr} + \lambda_{mq(\mathrm{unsat})} - \Delta\lambda_{mq} \tag{57}$$

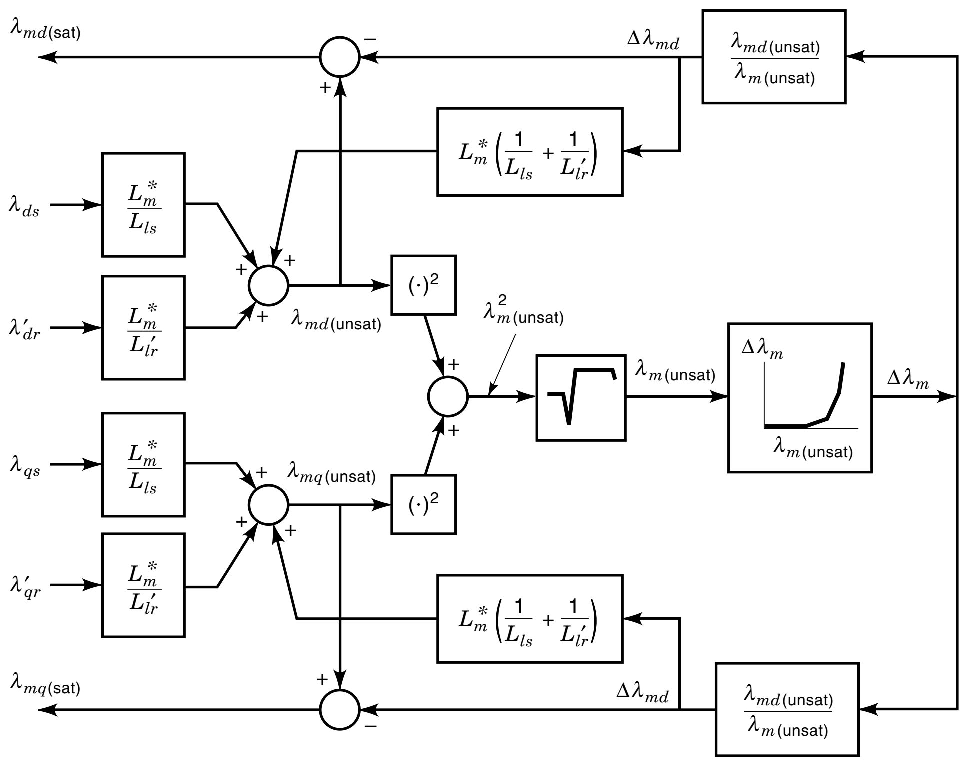

Figure 8. Block diagram for the procedure to calculate saturated air gap flux linkages $\lambda_{mq(\mathrm{sat})}$ and $\lambda_{md(\mathrm{sat})}$.

When combined with Eq. (24), the q-axis portion of unsaturated value of flux linkage is

$$\lambda_{mq(\mathrm{unsat})} = \left(\frac{1}{\dfrac{1}{L_m}+\dfrac{1}{L_{ls}}+\dfrac{1}{L'_{lr}}}\right) \left[\frac{\lambda_{qs}}{L_{ls}}+\frac{\lambda'_{qr}}{L'_{lr}}+\left(\frac{1}{L_{ls}}+\frac{1}{L'_{lr}}\right)\Delta\lambda_{mq}\right] \tag{58}$$

A similar result holds for the unsaturated value of d-axis air gap flux linkage. A block diagram showing the overall flow of signals to model induction motor saturation is given in Fig. 8 (8) where, for convenience, we have defined

$$L_m^* = \frac{1}{\dfrac{1}{L_m}+\dfrac{1}{L_{ls}}+\dfrac{1}{L'_{lr}}} \tag{59}$$

SIMULATION OF DEEP BAR EFFECT

Another very important phenomenon in squirrel cage induction machine concerns the uneven distribution of currents in the rotor bars, termed deep bar effect. Because a filament of current experiences a greater inductance at the bottom of the bar than on the top portion, the current tends to rise to the top of the bar facing the air gap, resulting in greater torque as well as higher losses at a given slip frequency. This phenomenon is frequently used to improve the starting performance of a squirrel cage machine since the effect is greatest under the starting condition due to the fact that the bar reactance is greatest at this point.

Simulation of the deep bar phenomenon is readily accomplished by breaking up all of the bars of the rotor into equal layers. The machine can then be simulated by modeling the equations defining the circuit of Fig. 9. A treatment of modeling of machines with deep bar effect is given in (9). A method to establish the parameters of the equivalent circuit of Fig. 9 is given in (10).

SATURATION MODEL WITH CURRENTS AS STATE VARIABLES

In recent years, numerous papers have been written concerning the simulation of saturated induction machines proposing the use of currents as the model state variables [e.g., (11–

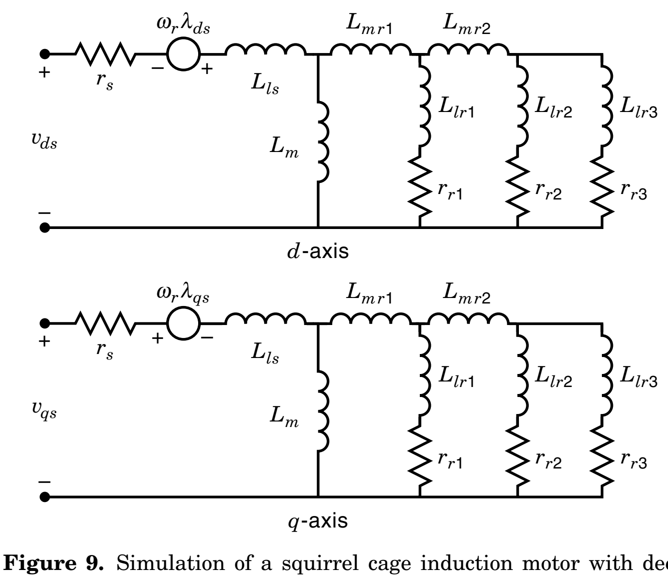

Figure 9. Simulation of a squirrel cage induction motor with deep bar effect modeled with three bar sections—rotor reference frame.

13)]. In the process of analysis, a so-called cross-saturation phenomenon has been identified which was supposedly neglected prior to this time. In reality, prior to 1981, flux linkages rather than currents were used to model core saturation primarily to avoid the difficulties addressed in these references. It has been demonstrated that the solution of the two methods are identical (8). Because of the complexity of the simulation (involving inversion of a 4 × 4 matrix every time step), the method is not recommended.

SIMULATION OF SYNCHRONOUS MACHINE

Wound field and permanent magnet synchronous machines can be modeled by use of the same d–q–0 transformation used for induction machines. However, in this case, since the rotor is not symmetric, wound field machines must be modeled in a reference frame rotating with the asymmetry (i.e., a reference frame rotating with the rotor) in order to simplify the coupled equation which exists in phase variable form. The d–q–0 differential equations depicting behavior of a wound field synchronous machine are

$$v_{qs} = r_s i_{qs} + \frac{d\lambda_{qs}}{dt} + \omega_r \lambda_{ds} \tag{60}$$

$$v_{ds} = r_s i_{ds} + \frac{d\lambda_{ds}}{dt} - \omega_r \lambda_{qs} \tag{61}$$

$$0 = r'_{qr} i'_{qr} + \frac{d\lambda'_{qr}}{dt} \tag{62}$$

$$0 = r'_{dr} i'_{dr} + \frac{d\lambda'_{dr}}{dt} \tag{63}$$

$$v'_{fr} = r'_{fr} i'_{fr} + \frac{d\lambda'_{fr}}{dt} \tag{64}$$

The dr and qr circuits are called the amortisseur windings (“killer” or damper windings) and are physically realized by a shorted squirrel cage constructed in much the same manner as the squirrel cage of an induction machine (often labeled as kd and kq). The last equation corresponds to the excited rotor field winding. Primes are again used as a reminder that the rotor circuits have been referred to the stator by the appropriate turns ratio. Note that Eqs. (60–63) are identical in form to the induction motor equation except that the speed of the reference frame ω has been set equal to the speed of the rotor ω_r, and that the rotor has asymmetry ($r_{qr} \neq r_{dr}$).

The flux linkages are related to the currents by

$$\lambda_{qs} = L_{ls} i_{qs} + L_{mq}(i_{qs} + i'_{qr}) = L_{ls} i_{qs} + \lambda_{mq'} \tag{65}$$

$$\lambda'_{qr} = L'_{lqr} i'_{qr} + L_{mq}(i'_{qr} + i_{qs}) = L'_{lqr} i'_{qr} + \lambda_{mq'} \tag{66}$$

$$\lambda_{ds} = L_{ls} i_{ds} + L_{md}(i_{ds} + i'_{dr} + i'_{fr}) = L_{ls} i_{ds} + \lambda_{md} \tag{67}$$

$$\lambda'_{dr} = L'_{ldr} i'_{dr} + L_{md}(i_{ds} + i'_{dr} + i'_{fr}) = L'_{ldr} i'_{dr} + \lambda_{md} \tag{68}$$

$$\lambda'_{fr} = L'_{lfr} i'_{fr} + L_{md}(i_{ds} + i'_{dr} + i'_{fr}) = L'_{lfr} i'_{fr} + \lambda_{md} \tag{69}$$

An equivalent circuit of this machine can be established from these equations as shown in Fig. 10. These equations can be solved for the currents and air gap flux linkages as

$$i_{qs} = \frac{\lambda_{qs} - \lambda_{mq}}{L_{ls}} \tag{70}$$

$$i'_{qr} = \frac{\lambda'_{qr} - \lambda_{mq}}{L'_{lqr}} \tag{71}$$

$$i_{ds} = \frac{\lambda_{ds} - \lambda_{md}}{L_{ls}} \tag{72}$$

$$i'_{dr} = \frac{\lambda'_{dr} - \lambda_{md}}{L'_{ldr}} \tag{73}$$

$$i'_{fr} = \frac{\lambda'_{fr} - \lambda_{md}}{L'_{lfr}} \tag{74}$$

$$\lambda_{md} = L^*_{md}\left(\frac{i_{ds}}{L_{ls}} + \frac{i'_{dr}}{L'_{ldr}} + \frac{i'_{fr}}{L'_{lfr}}\right) \tag{75}$$

$$\lambda_{mq} = L^*_{mq}\left(\frac{i_{qs}}{L_{ls}} + \frac{i'_{qr}}{L'_{ldr}}\right) \tag{76}$$

where

$$L^*_{md} = \frac{1}{\dfrac{1}{L_{md}} + \dfrac{1}{L'_{ldr}} + \dfrac{1}{L'_{lfr}}} \tag{77}$$

$$L^*_{mq} = \frac{1}{\dfrac{1}{L_{mq}} + \dfrac{1}{L'_{lqr}}} \tag{78}$$

The equation for the electromagnetic torque is the same as for the induction machine, Eq. (28) but not Eq. (29), because of the nonsymmetrical rotor. A block diagram showing flow of data for purposes of simulation is shown in Fig. 11.

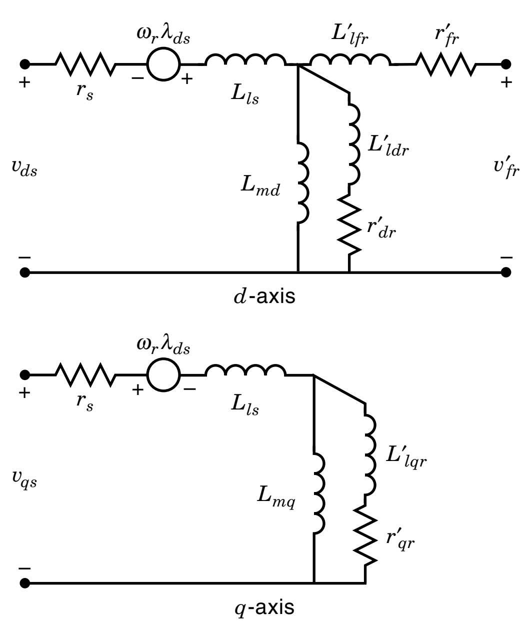

Figure 10. d–q–0 equivalent circuit of a wound field synchronous machine.

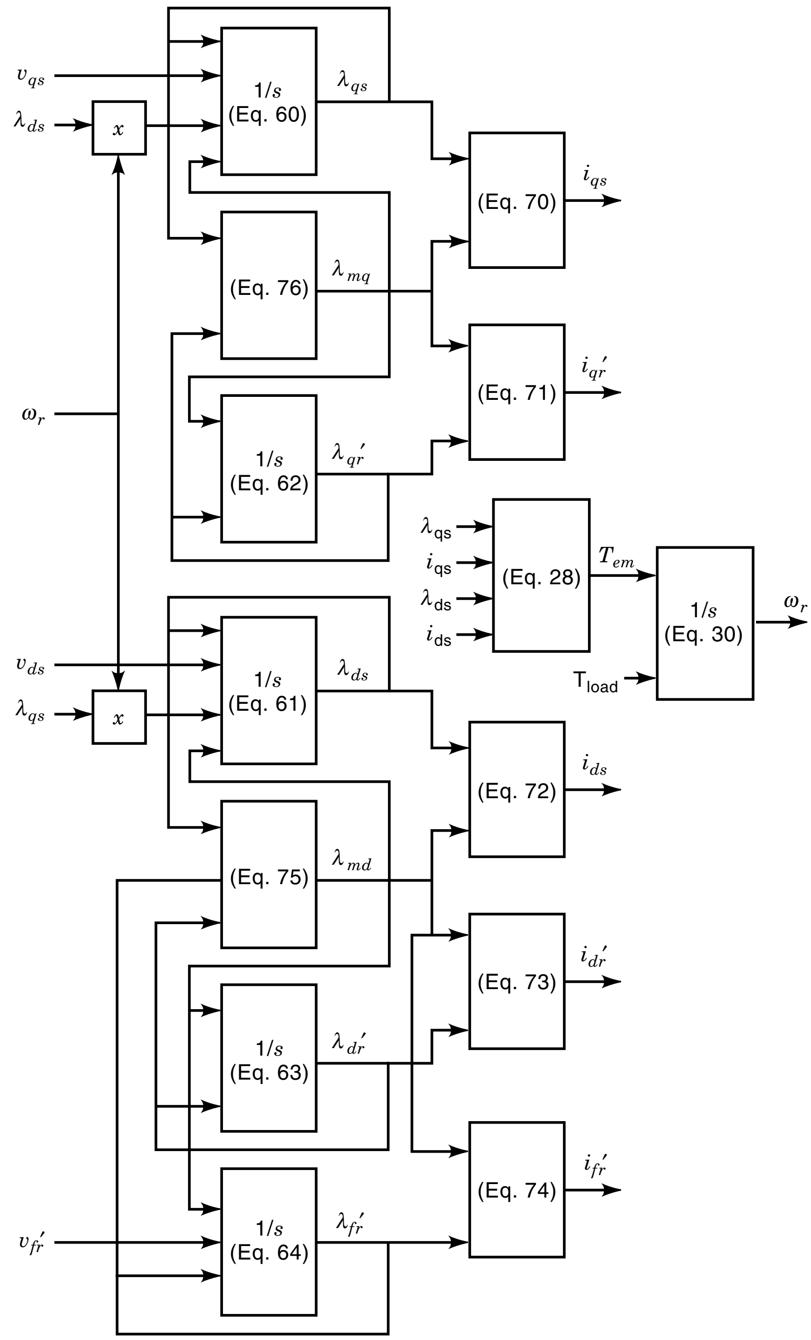

Figure 11. Simulation flow diagram for wound field synchronous machine.

It should be mentioned that the circuit of Fig. 11 is adequate only when predicting stator currents but fails when accurate portrayal of the rotor currents is desired. In this case, more detailed models are required which include the fact that there exists a flux component which links both the d-axis damper winding and field winding which does not enter the air gap and, therefore, does not link the stator windings. In this case, the reader is referred to (14).

SATURATION MODEL OF WOUND FIELD SYNCHRONOUS MACHINE

Because of the heavy excitation current (ampere turns) usually employed, saturation normally occurs first within the field poles of a salient pole synchronous machine. Hence, saturation becomes primarily determined by the flux in only one of the two magnetic axes (d–q axes), namely the d-axis. Derivation of the unsaturated flux linkage versus saturated flux linkage characteristic is done in the same manner by obtaining first the open circuit saturation curve (see Fig. 7). Derivation of the equations expressing saturation in this case is very simple but follows the induction machine example explained earlier. A block diagram of the resulting equations is shown in Fig. 12.

In cases where saturation occurs in the stator rather than, or in addition to, the rotor, the effect must be modeled by several saturation functions. A good discussion of this problem is given in (15). High-speed synchronous motors and tur-

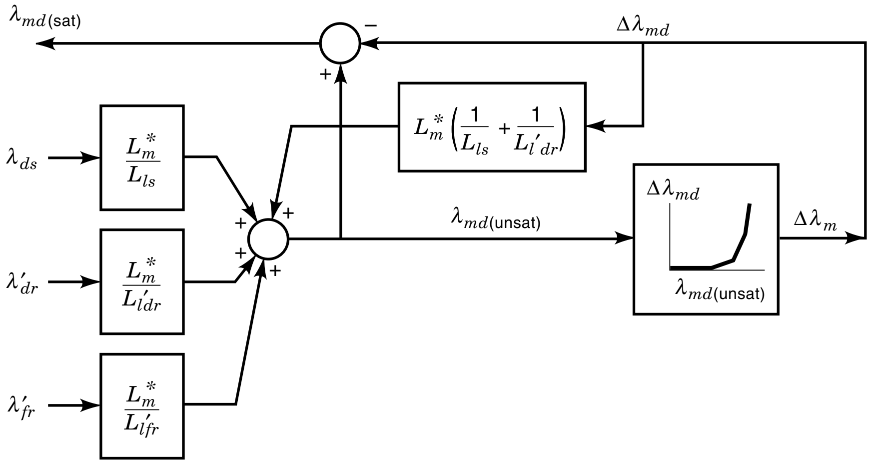

Figure 12. Saturation model for a salient pole wound field synchronous machine.

bogenerators are constructed with a round rotor which is typically not laminated. Because of the eddy currents which flow in the rotor body, the saturation phenomenon is complicated. While saturation is often still modeled as in Fig. 12, a more detailed model is needed for good correlation with physical tests. Reference 16 is a good beginning point.

OTHER MACHINES

While emphasis has been placed on the three-phase squirrel cage induction and salient pole wound field synchronous machines, many of the other common machines are close relatives of these two basic machine types. For example, a single-phase induction machine is, effectively, a two-phase induction machine with an unequal number of turns in the two phases. Simulation of this machine closely follows the d–q model presented in Fig. 4 with a turns ratio correction on the auxiliary winding to yield the equivalent of a balanced two-phase induction motor. Details of the derivation are given in (17). Permanent magnet motors can be modeled by using the synchronous machine d–q model with the d-axis circuit modified, as shown in Fig. 13. In this case, since a ferrite or rare-earth magnet has a relative permeability nearly that of air, L_{mag} represents the inductance due to the magnet itself. The inductance $L_{l\text{mag}}$ accounts for the leakage flux produced by the magnet but can be neglected since the magnet, itself, is modeled as a current source. If the rotor of the machine is not equipped with a cage, the cage windings can be simply removed from the circuit and their corresponding circuit equations eliminated. In this case, it is even possible to simulate the machine in a nonrotating (stationary) frame of reference. Reference 18 is a good place to begin concerning simulation of permanent magnet machines.

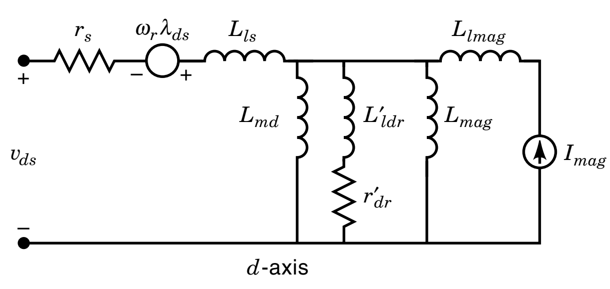

Figure 13. Equivalent d-axis circuit for three-phase permanent magnet machine.

Finally, various types of reluctance machines are also related to the synchronous machine. The synchronous-reluctance machine has a conventional three-phase stator structure similar to an induction or synchronous machine but has a special rotor to enhance the reluctance torque produced by a salient pole rotor structure. The equivalent circuit and its modeling is the same as a wound field synchronous machine except that the field winding is omitted. The variable reluctance machine is unusual in that it has both a salient pole stator and a rotor thereby invalidating the common development of all of the other ac machines up to this point. The subject is a special one to which the reader is referred to the literature. If simulation techniques for this machine are of particular importance, (19) is a recommended starting point. Three books that treat the overall subject of analysis and simulation of ac machines in some detail are listed as (20–22).

BIBLIOGRAPHY

1. V. Bush, F. D. Gage, and H. R. Stewart, A continuous integraph, *Franklin Inst. J.,* **203**: 63–84, Jan. 1927.
2. L. Teplow, Stability of synchronous motors under variable-torque loads as determined by the recording product integraph, *Gen. Elec. Rev.,* **31** (7): 356–365, July 1928.
3. R. H. Park, Two-reaction theory of synchronous machines, Part 1—Generalized method of analysis, *AIEE Trans.,* **48**: 716–727, 1929.
4. H. C. Stanley, An analysis of the induction motor, *AIEE Trans.,* **57** (Supplement): 751–755, 1938.
5. P. C. Krause, T. A. Lipo, and D. P. Carroll, Applications of analog and hybrid computation in electric power system analysis, *Proc. IEEE,* **62**: 994–1009, 1974.
6. C. H. Thomas, Discussion of "Analogue Computer Representation of Synchronous Generators in Voltage Regulation Studies" by M. Riaz, *Trans. AIEE (Power Apparatus and Systems),* **75**: 1182–1184, 1956.
7. P. C. Krause and C. H. Thomas, Simulation of symmetrical induction machinery, *IEEE Trans. Power Appar. Syst.,* **PAS-84**: 1038–1053, 1965.
8. M. Osama, K. Sakkoury, and T. A. Lipo, Transient behavior comparison of saturated induction machine models, *IMACS-TC1-93,*

(Computational Aspects of Electromechanical Energy Converters and Drives), 577–584, 7–9 July, 1993.

9. E. A. Klingshirn and H. E. Jordan, Simulation of polyphase induction mchines with deep rotor bars, *IEEE Trans. Power Appar. Syst.,* **PAS-89**: 1038–1043, 1970.
10. W. H. Creer, D. W. Novotny, and T. A. Lipo, Determination of equivalent circuits for induction machines with skin effect using terminal characteristics, *Electric Machines and Power Systems,* **10** (4–5): 379–394, 1985.
11. P. Vas, Generalized analysis of saturated a.c. machines, *Archiv fur Elektrotechnik,* **64**: 57–62, 1981.
12. P. Vas, K. E. Hallenius, and J. E. Brown, Cross-saturation in smooth air gap electrical machines, *IEEE Trans. Energy Convers.,* **EC-1**: 103–109, 1986.
13. J. A. A. Melkebeek, Magnetising-field saturation and dynamic behaviour of induction machines, Part 1: Improved calculation method for induction-machine dynamics, *IEE Proc.,* **130**, Pt. B (No. 1): 1–9, Jan 1983.
14. I. M. Canay, Causes and discrepancies on calculation of rotor quantities and exact equivalent diagram of synchronous machines, *IEEE Trans. Power Appar. Syst.,* **PAS-88**: 1114–1120, 1969.
15. G. R. Slemon, Analytical models for saturated synchronous machines, *IEEE Trans. Power Appar. Syst.,* 409–417, 1971.
16. R. P. Schultz, W. D. Jones, and D. N. Ewart, Dynamic models of turbine generators derived from solid rotor equivalent circuits, *IEEE Trans. Power Appar. Syst.,* **PAS-92**: 926–933, 1973.
17. P. C. Krause, Simulation of unsymmetrical 2-phase induction machines, *IEEE Trans. Power Appar. Syst.,* **PAS-84**: 1025–1037, 1965.
18. P. Pillay and R. Krishnan, Modeling, simulation and analysis of permanent magnet motor drives, Part I: The permanent magnet synchronous motor drive, *IEEE Trans. Ind. Appl.,* **25**: 265–273, 1989.
19. T. J. E. Miller, *Switched Reluctance Motors and Their Controls,* Hillsboro, OH: Magnaphysics Publishing, 1993.
20. C. M. Ong, *Dynamic Simulation of Electric Machinery Using Matlab / Simulink,* Upper Saddle River, NJ: Prentice-Hall, 1998.
21. P. C. Krause, O. Wasynczuk, and S. Sudhoff, *Analysis of Electric Machinery,* Piscataway, NJ: IEEE Press, 1995.
22. D. W. Novotny and T. A. Lipo, *Dynamics and Vector Control of Induction Motor Drives,* London: Oxford Press, 1996.

T. A. LIPO
University of Wisconsin